Comparison on Experimental and Numerical Results for Helical Swimmers inside Channels

Ahmet Fatih Tabak, Fatma Zeynep Temel, and Serhat Yesilyurt, *Member, IEEE*

Abstract—**Swimming micro robots are becoming feasible in biomedical applications such as targeted drug delivery, opening clogged arteries and diagnosis owing to recent developments in micro and nano manufacturing technologies. It has been demonstrated at various scales that micro helices with magnetic coating or attached to a magnet can move in fluids with the application of external rotating magnetic fields. The motion of micro swimmers interacting with flow inside channels needs to be well understood especially for medical applications where the motion of micro robots inside arteries and conduits in the body become pertinent. In this work, swimming of helical micro robots with magnetic heads inside tubes is modeled with the resistive force theory (RFT) and validated with experiments conducted in glycerin filled mini glass channels placed in rotational magnetic fields. The time-averaged forward velocities of magnetically driven micro swimmers that are calculated by the RFT model agree very well with experimental results.**

Keywords-swimming micro robot, helical wave propagation, rotating magnetic field actuation, resistive force theory, wall effects

I. INTRODUCTION

RECENT developments in MEMS (micro electro mechanical systems) and nano-technology rendered bioinspired medical swimming micro robots realizable [1, 2, 3, 4]. Zhang *et al.* [5, 6] manufactured a helical filament from GaAs with dimensions of 1.8 µm in width, 30 µm in length and 200 nm in thickness and attached to a soft magnetic nickel on one side. Authors demonstrated that the structure moves in the direction of its helical axis with the application of a rotational magnetic field in that direction. They pointed out that the linear swimming velocity is affected not only by the size of the head, but also the strength of applied magnetic field. Ghosh and Fischer [7] manufactured and operated chiral colloidal propellers having 200-300 nm width and 1-2 µm length made of silicon dioxide and a thin layer of ferromagnetic material (cobalt) deposited on one side. Those magnetic nano-structured propellers were, then, navigated in water with micrometer-level precision using rotational magnetic fields.

In-channel experiments are especially significant for their relevance to in vivo applications since it is crucial to control the micro robots injected in and navigated back from channels in human body such as arteries, capillaries and similar

Authors are with the Faculty of Natural Sciences and Engineering, Sabanci University, Orhanli, Tuzla, 34956 Istanbul, Turkey
(e-mail: tabak@sabanciuniv.edu,zeyneptemel@sabanciuniv.edu, syesilyurt@sabanciuniv.edu).
First two authors have contributed equally in this work.

conduits to accomplish medical operations. Honda *et al.* [8] used external actuation by rotating magnetic field to obtain propagation of a cm-long spiral swimming robot in a silicon oil filled 15-mm diameter channel. Authors demonstrated that the motion of the robot is in a linear relationship with excitation frequency and results agreed well with Sir Lighthill's [9] slender body theory results.

Micro-robotic operations require mathematical models to predict and control in vivo performance with high precision. Analytical studies on micro swimmers with helical waves, free and near solid boundaries or confined to channels are carried out for over decades. Gray and Hancock [10] studied the fluid forces on the whip-like tail of Sea Urchin spermatozoa with resistive force coefficients to implement a linear relationship between slender-body motion and fluid drag, also known as Resistive Force Theory (RFT). Brennen and Winet [11] studied the effects of structural geometry on fluid forces and discussed the effect of solid walls on resistive force coefficients. They introduced modified coefficient sets for finite-length slender cylinders based on orientation of motion with respect to solid boundaries. Blake [12] discussed that the ratio between resistive force coefficients are subjected to the proximity to the solid boundary. Lauga *et al.* [13] modeled the motion of E. *Coli* near a flat plate with resistive force coefficients and confirmed the resultant circular trajectory with experiments. Higdon [14] discussed the fluid forces, propulsive effect and efficiency of helical wave propagation on bacterial tails. Felderhof [15] invoked Stokes equation with perturbation methods for planar and helical wave propagating swimmers of infinite length moving inside a cylindrical channel. Manghi *et al.* [16] presented their work on a rotating elastic nano-length filaments and resultant propulsive effect solving for thermal, hydrodynamic, and structural effects with Rotne-Prager Green functions.

In this work we conducted experiments with magnetically driven single-link micro robots fully submerged inside a narrow cylindrical glass tube filled with viscous fluid. Strength of the rotating magnetic field is modified by current control of Helmholtz coils. Displacements of the robots along the channel axis are captured with a camera. Moreover, a 6-dof time-dependent hydrodynamic model is built based on RFT including: a novel technique to implement cylindrical channel effects, and magnetic step-out frequency phenomena. Experimental results are used to validate the proposed hydrodynamic model with appropriate tuning of body resistance coefficients due to irregular shapes of the magnetic heads and the overall flow conditions that differ

from simple viscous drag on the body, which is commonly used to obtain analytical body resistance coefficients. Numerical and experimental data for time-averaged forward velocity are found to agree well.

II. METHODOLOGY

In this section one-link micro swimmer robot fabrication procedure, experimental setup essentials, and coupled mathematical model for magnetically actuated micro swimmer robots are discussed in detail.

A. Fabrication of Micro Swimmers

Micro robots consist of a permanent magnetic head and a non-magnetic metal helical wire tail. Magnetic head is the element that rotates together with the rotating magnetic field. Lumps of neodymium-iron-boron ($Nd_2Fe_{14}B$) magnet particles about 160 µm in diameter are used to have relatively high magnetization factors in small volumes, remanence of the particles are estimated as 1.2 T. Each robot has approximately same size of magnetic particles with minor differences due to the irregularity of the lumps. Magnetic head is attached to the helical tail with a strong adhesive so that they move together. Tails are manually manufactured from copper wires of 110 µm diameter: wires are wound around thicker ones and deformed plastically to adjust the pitch of helices. Table I shows the dimensions of metal helices used in the experiments.
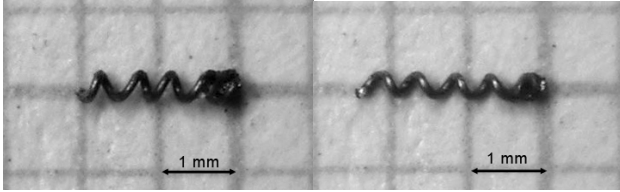

Fig. 1. Helical swimmers used in the experiments: a) L2W3; b) L2W4.

TABLE I
DIMENSIONS OF MICRO SWIMMERS

	Length [mm]	Number of waves	Tail length [mm]	Diameter of head [mm]	Helix diameter [mm]
L2W3	2.17	3	1.71	0.46	0.41
L2W4	2.45	4	2.09	0.36	0.36

B. Experimental Setup

Helical swimmers are placed in 10-cm long glass pipettes of 1-mm-inner diameter, filled with glycerol and sealed at both ends. Pipettes are placed on the **x**-axis of the setup shown schematically in Fig. (2).

Orthogonal electromagnetic coil pairs such as Helmholtz coils are used to obtain the rotating magnetic field, which emerges as the choice of propulsion and steering for helices attached to magnetic particles as untethered swimming micro robots [2, 5, 6, 8, 9, and 17]. One pair of coils is placed on the **z**-axis and other is placed on **y**-axis perpendicularly to the other as seen in Fig. (2). Electromagnetic coil pairs used in experiments are not identical and dimensions are given in

Table II. Helmholtz coil pairs are mounted as shown in Fig. (2). Alternating currents are applied to coils in order to obtain two independent magnetic fields, which are perpendicular to each other with a phase shift and form a rotating magnetic field. Currents applied to the small (in the z-direction) and big (in the y-direction) coils are defined as $I_{SC} = I_{0,SC} \times \sin(2\pi ft)$ and $I_{BC} = I_{0,BC}\sin(2\pi ft)$ respectively.
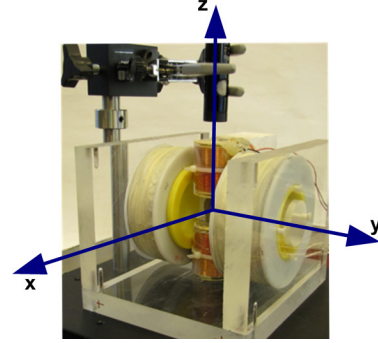

Fig. 2. Experimental setup consists of electromagnetic coil pairs and USB microscope camera

TABLE II
DIMENSIONS OF COILS

Coils	y axis	z axis
Measured resistance [Ω]	14	7.5
Wire diameter [mm]	0.45	0.8
Number of turns	ca 1400	ca 750
Coil diameter [mm]	30	90
Distance between coils [mm]	20	60

The current is transmitted to the coils from power supplies via Maxon ADS_E 50/10 motor drives that are connected to DS1103PPC controller board. Maxon motor drives are operated with dSPACE and the signal is converted from digital to analog. The magnitude and frequency of the sinusoidal currents are adjusted by the ControlDesk software. Forward swimming of helices is observed with TIMM-400 S/W v. 0.1-100 Microscope having a resolution of 720 x 576 pixels in which a USB digital camera that can record maximum 30 frames per second is mounted. Each coil is driven by a dedicated Maxon motor drive controlled within Simulink environment [18].

C. Mathematical Model

1) Equation of Motion

Linear and angular velocities and trajectory of helical swimmers are obtained from the solution of the equation of motion with the propulsion force due to the rotation of the tail when the external magnetic torque is applied, total drag force and drag torque on the swimmer as follows:

$$\mathbf{F}_d + \mathbf{F}_p = \mathbf{0}$$
$$\mathbf{T}_d + \mathbf{T}_{ext} = \mathbf{0}$$
(1)

Here subscripts *p*, *d* and *ext* denote propulsion, drag and the external effects respectively.

Force and torque vectors due to hydrodynamic propulsion and fluid drag are constructed by the resistive force theory

[10]: the force and torque vectors are obtained from the linear and angular velocity vectors with a linear resistance relationship as follows:

$$\begin{bmatrix} \mathbf{F}_d + \mathbf{F}_p \\ \mathbf{T}_d \end{bmatrix} = (\mathbf{B}_t + \mathbf{B}_h) \begin{bmatrix} \mathbf{U} \\ \mathbf{\Omega} \end{bmatrix} \quad (2)$$

where 'U' and '$\mathbf{\Omega}$' are linear and angular velocity vectors in swimmer frame, and '$\mathbf{B}_t$' and '$\mathbf{B}_h$' are 6-by-6 resistance matrices for the helical tail and the magnetic body respectively [19]. The resistance matrix for a rigid helical tail decomposes as follows:

$$\mathbf{B}_t = \int_0^L \begin{bmatrix} \mathbf{RCR'} & -\mathbf{RCR'S} \\ \mathbf{SRCR'} & -\mathbf{SRCR'S} \end{bmatrix} ds \quad (3)$$

where L is the apparent tail length, s is the spatial s-coordinate in the swimmer frame, $\mathbf{R}$ is the rotation between the local Frenet-Serret frame on the helical tail [20] and the swimmer frame, $\mathbf{S}$ is the skew-symmetric matrix for the cross products between the position and velocity vectors in the swimmer frame, the diagonal matrix $\mathbf{C}$ is the local resistance matrix on the tail, and superscript ''' denotes transpose.

Due to the angular symmetry of the cylindrical cross section of the tail, normal and binormal components of the local resistive force are proportional to the normal and binormal components of the local velocity with the same normal resistive force coefficient, which is given by [11]:

$$c_n = \begin{cases} \dfrac{4\pi\mu}{\ln(\lambda/d)+0.193-3\lambda/8h}, & \dfrac{\lambda}{2h} \leq 1 \\[3mm] \dfrac{4\pi\mu}{\ln(2h/d)}, & \dfrac{\lambda}{2h} > 1 \end{cases} \quad (4)$$

The tangential component of the resistive force is proportional to the velocity in that direction with the tangential resistive force coefficient [11]:

$$c_t = \begin{cases} \dfrac{2\pi\mu}{\ln(\lambda/d)-0.807-3\lambda/16h}, & \dfrac{\lambda}{2h} \leq 1 \\[3mm] \dfrac{2\pi\mu}{\ln(2h/d)}, & \dfrac{\lambda}{2h} > 1 \end{cases} \quad (5)$$

In (4) and (5), h is the minimum local distance of the center line of the tail to the surface of the channel, d is the tail radius, and λ is the helical pitch.

Resistance matrix for rigidly-attached head of the micro swimmer, $\mathbf{B}_h$, is given by:

$$\mathbf{B}_h = \begin{bmatrix} \mathbf{D} & -\mathbf{DW} \\ \mathbf{WD} & \mathbf{E} \end{bmatrix} \quad (6)$$

where $\mathbf{D}$ and $\mathbf{E}$ are diagonal 3-by-3 translational and rotational body drag coefficient matrices respectively, and $\mathbf{W}$ is the skew-symmetric matrix for the body center of mass. Resistance matrix given by (6) is modified in order to account for the wall effects as discussed next.

2) Wall Effects

Body and tail drag matrices given by (3) and (6) are modified in each time step in order to implement the presence of inflexible solid channel boundaries. Hard-constraint kinematic equations, i.e. in case of an elastic collusion between the micro swimmer's body and channel walls, are transformed into soft kinematic constraints for an imaginary concentric inner cylinder of radius (r_{ch} -ε) as follows:

$$\mathbf{\Psi}_{6\times6}\begin{bmatrix} \mathbf{U} \\ \mathbf{\Omega} \end{bmatrix} := \begin{cases} \begin{bmatrix} \mathbf{R}_\theta\left(\mathcal{R}\mathbf{U}+\mathbf{\Omega}\times\mathbf{p}\right) \\ \mathbf{R}_\theta\left(\mathbf{\Omega}\times\mathbf{p}\right) \end{bmatrix}, & \|\mathbf{p}\| \neq 0 \\[3mm] \mathbf{0}_{6\times6} & , \|\mathbf{p}\| = 0 \end{cases} \quad (7)$$

where $\mathbf{\Psi}$ is the constraint matrix, $\mathcal{R}$ is the matrix handling rotations from swimmer frame to stationary lab frame, i.e. **xyz,** determined by integrating time dependent quaternion rotations [21], and $\mathbf{R}_\theta$ is the transformation matrix between lab coordinate systems, i.e. from **xyz** to **xrθ** coordinates.

The vector **p** in (7) represents the position of surface points of the swimmer with respect to swimmer's center of mass, and is set to zero unless the proximity of the swimmer to channel wall exceeds the limit such that body surface touches or penetrates the imaginary concentric inner cylinder. In effect, $\mathbf{\Omega}\times\mathbf{p}$ is used to consider the contact torque on the swimmer. If the limit is exceeded, nonzero elements within $\mathbf{\Psi}$ modify the elements of resistance matrix as follows:

$$\mathbf{B}'_{h,ij} = \begin{cases} \dfrac{k}{(\varepsilon-\delta)/\varepsilon}\mathbf{B}_{h,ij}, & \mathbf{\Psi}_{ij} \neq 0 \\[3mm] \mathbf{B}_{h,ij}, & \mathbf{\Psi}_{ij} = 0 \end{cases} \quad (8)$$

where δ is the penetration depth of the swimmer in **xrθ** coordinates as depicted in Fig. (3), and k is the stiffness tuning parameter which is 30 unless otherwise stated.
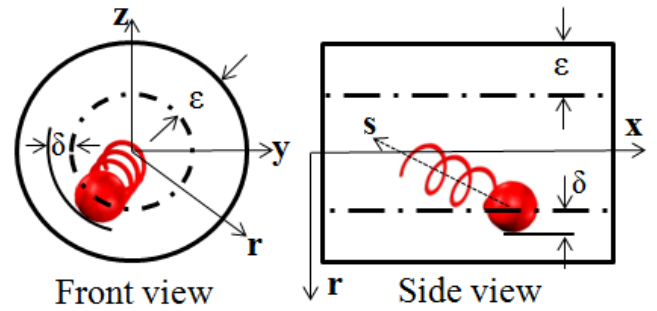

Fig. 3. Swimmer body penetrating imaginary inner concentric cylinder: Penetration depth δ is computed in **r**-coordinate of the lab frame.

Eq. (8) ensures that as the minimum distance decreases, the corresponding resistance matrix elements are multiplied with a large scalar to constrain the motion in that direction. The artificial concentric inner cylinder is fixed as $\varepsilon = r_{ch}$ /2 in order to impose the effect of channel walls on the swimmer body gradually. However, the resistance matrix must have full rank at all times, i.e. det($\mathbf{B}_h + \mathbf{B}'_t)\neq0$.

3) Magnetic Torque

External torque vector in (1) happens due to the magnetic field applied along the **x**-axis in lab frame. Magnitude of the magnetic field, **H,** along the axis of a single coil is proportional to the current passing through that coil, and given by [22]:

$$\|\mathbf{H}\| = \frac{NIa^2}{2\left(a^2 + l^2\right)^{1.5}} \tag{9}$$

where N is the number of turns, I is the magnitude of the current, a is the radius of the coil, l is the distance from the coil.

The resultant torque felt by the magnetic head of the swimmer is given by:

$$\mathbf{T}_{ext} = \mathcal{R}\,'\mu_{eff} V \|\mathbf{M}\|\|\mathbf{H}\|\mathbf{n}_x \sin(\gamma) \tag{10}$$

where V is the volume, μ_{eff} is the actual permeability, and **M** is the magnetization vector of the magnetic head. The direction of the resultant torque is denoted by the normal vector $\mathbf{n}_x$. Angle between the external magnetic field and the body is denoted by γ and computed as the integral of the difference between the angular velocities of body and rotational magnetic field:

$$\gamma = \int_0^t \left(2\pi f - \Omega_s\right) dt' \tag{11}$$

where f is the actuation frequency of the magnetic field, and Ω_s is the resultant swimmer rotation along **s**-axis, which is initially 0 and updated at each simulation time step beforehand (1) is solved. This consequently results in $\mathbf{F}_p$ in (1) due to cross-coupling terms in resistance matrix given by (3). In the case when the swimmer rotates with the frequency of the magnetic field the angle γ remains constant, however, when the strength of the field is not enough to overcome the fluid's resistance it varies with time.

Continuous steady torque is sustained by means of the rotating magnetic field as long as the swimmer rotates with the field. When the swimmer loses its synch with the magnetic field, effective torque drops and swimmer can no longer rotate at the same rate with the field, thus, the propulsion becomes erratic. The maximum frequency that the swimmer can follow without loss of propulsion is called step-out frequency.

III. Results

Helical swimmers are placed inside the glass pipettes with inner diameters of 1 mm and filled with glycerol having a dynamic viscosity of 0.1 Pa·s. At 10 Hz, Reynolds numbers for both head and helical tail are calculated as Re_{head_L2W3} $=2.4 \times 10^{-3}$, $\mathrm{Re}_{tail\_L2W3} = 12.8 \times 10^{-3}$, $\mathrm{Re}_{head\_L2W4} = 2.4 \times 10^{-3}$, and $\mathrm{Re}_{tail\_L2W4} = 18.1 \times 10^{-3}$ where ρ, V, r, η, f, d and A are density of the fluid, linear velocity of micro swimmer, radius of head, viscosity of the fluid, rotation frequency, diameter of the tail and amplitude of helical tail wave, respectively. Thus inertial effects are negligible with respect to viscous forces

for both the forward motion of the head and the rotation of the tail.

RFT based model simulations are carried out for 25 complete periods of the rotation of the external magnetic field. Equation of motion (1) is solved by Adams-Bashforth-Moulton PECE solver [23]. Each simulation took about 15 to 45 seconds on a single processor of 64-bit Linux workstation with dual quad-core Xeon processors clocked at 2.6 GHz depending on the numerical stiffness of the swimmer's motion. Time-averaged forward velocities of the swimmers are calculated over the entire duration of the motion. The experimental time-averaged **x**-direction velocity is calculated by dividing the traveled distance to the travel time of micro swimmer.

Similar behavior is observed for both swimmers L2W3 and L2W4 for forward velocities in lab frame. The linear velocity is proportional to the actuation frequency up to the step-out frequency. In the linear region, rotations of the magnetic field and the swimmer are identical, and the magnetic torque on the swimmer is steady. As the magnetic actuation frequency increases, time-averaged forward velocity decreases due to loss of useful magnetic torque, which is inapt to enforce the swimmer follow continuously with the frequency of rotating magnetic field. As depicted in Fig. (4), at times the swimmer reverses rotational direction as the cross product of the magnetization of the head and the external field points at the opposite direction, slows down the swimmer, and, even forces the swimmer to move in the opposite direction.
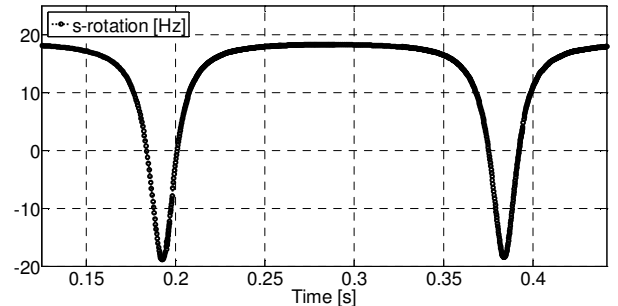

Fig. 4. Simulation based rotational **s**-velocity: Effect of step-out frequency and spontaneous counter-rotation of L2W4; operating at 6.85 mT with $f = 20$ Hz.

Figures (5)-(6) show the comparison of time-averaged **x**-velocities observed by experiments and computed by RFT based model for micro swimmer robot designated as L2W3 operating with two different magnetic field strengths, i.e. 6.85 mT and 7.22 mT. Simulation results are in good agreement with experiments. They predict the linear relationship between magnetic actuation frequency and time-averaged forward velocity till step-out frequency occurs. After that point onward, consequent nonlinear decrease in forward velocity is partially predicted in all cases as shown in Figs. (5)-(6). It is noted that, linear and rotational **s**-drag coefficients of swimmer body are multiplied with 0.3 and 1.15, respectively, in order to predict the time-averaged forward velocity of L2W3. Moreover, tuning of body drag coeffi-

cients in simulations is only to compensate the effects of possible morphological impurities of the body in experiments; nevertheless, this procedure does not affect the linear behavior shown in Figs. (5)-(8). Lastly, to predict the step-out frequency with minimum magnetic torque, magnetization of the head is divided by 1.35 for this robot: in effect, that factor accounts for the angle between the magnetic field and the magnetization.
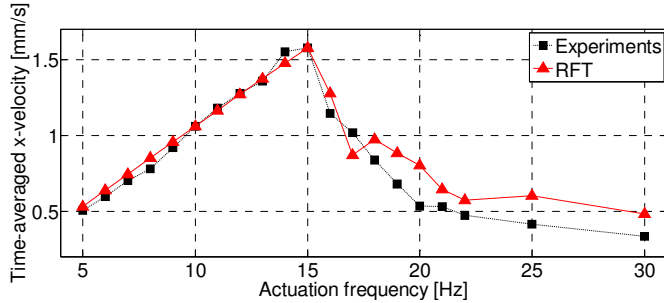

Fig. 5. Time-averaged **x**-velocity vs. magnetic actuation frequency. Experiment vs. RFT for L2W3 at 6.85 mT
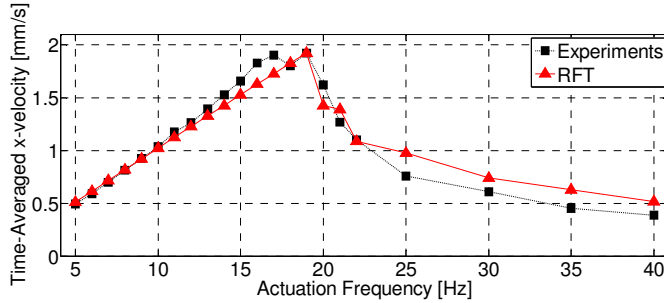

Fig. 6. Time-averaged **x**-velocity vs. magnetic actuation frequency. Experiment vs. RFT for L2W3 at 7.22 mT

Figures (7)-(8) show the comparison of time-averaged **x**-velocities observed by experiments and computed by RFT based model for micro swimmer robot designated as L2W4 operating under same magnetic field strengths with L2W3. Simulation results predict the linear relationship between magnetic actuation frequency and time-averaged forward velocity with high accuracy till step-out frequency occurs. Similarly to L2W3 results, consequent nonlinear decrease in forward velocity is partially predicted in all cases as shown in Figs. (7)-(8). It is noted that, linear and rotational **s**-drag coefficients of body is multiplied with 3 and 1.1, respectively, in order to predict the time-averaged forward velocity of L2W4. Lastly, magnetization of the head is divided by 1.49 in order to account for the actual magnetic torque based on the step-out frequency for this robot.
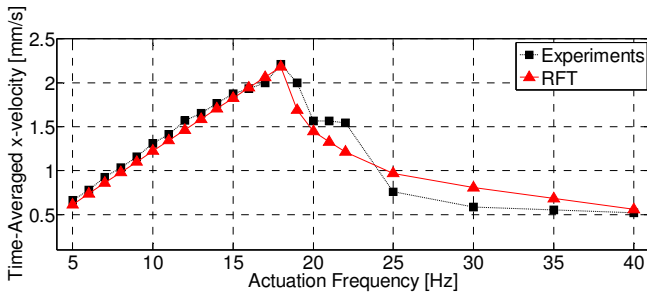

Fig. 7. Time-averaged **x**-velocity vs. magnetic actuation frequency. Experiment vs. RFT for L2W4 at 6.85 mT

Figure (9) demonstrate the wall effects on **yz**-trajectory of the swimmer as magnetic field frequency is smaller than step-out frequency. Implementation of soft constraints on inner cylinder actually limits the position of the micro swimmer on the **yz**-plane such that overall motion of the swimmer's center of mass is mostly restricted to artificial inner cylinder as it continuously penetrates and bounces back and remains on the wall (the trajectory illustrated with red in Fig. (9)). However, if (8) is not applied, swimmer follows a more monotonous path and does not remain inside the channel (green trajectory in Fig. (9)).
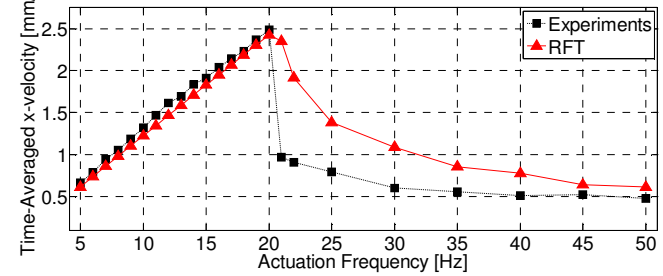

Fig. 8. Time-averaged **x**-velocity vs. magnetic actuation frequency. Experiment vs. RFT for L2W4 at 7.22 mT
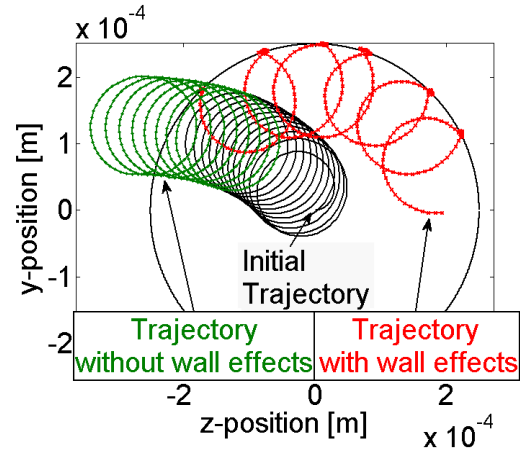

Fig. 9. Simulation based **yz**-trajectory for L2W4 operating at 7.22 mT with f = 20 Hz.

Figure (10) demonstrates the step-out phenomena on **yz**-trajectory of the swimmer as soft constraints are implemented. As the useful magnetic torque decreases and spontaneous inverse **s**-rotations occur as demonstrated by Fig. (4), swimmer loses forward thrust and momentarily pauses motion on **yz**- plane.

Figure (11) demonstrates the time dependent orientation of L2W3 with respect to channel long axis by means of two consecutive snap-shots while operating at 7.41 mT with f = 10 Hz in glycerol filled channel. Robots tend towards the channel wall as moving forward as predicted by RFT model.

Yawing towards the channel wall as demonstrated in Fig. (11) is also observed in simulations (see Fig. (9)). Since simulations do not account for the resultant flow within the channel or the gravitational torque on the swimmer, further study is needed in order to single out the origins of this behavior observed in experiments.
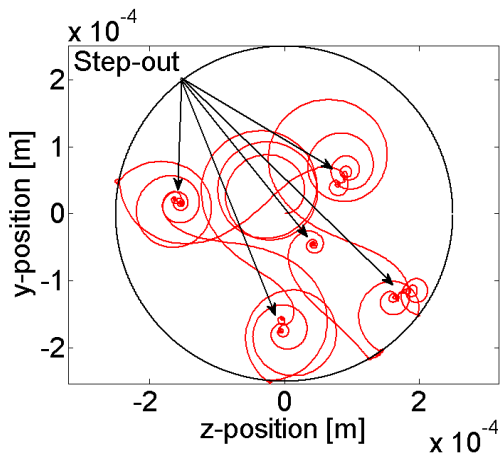
Fig. 10. Simulation based **yz**-trajectory for L2W4 operating at 6.85 mT with f = 20 Hz.
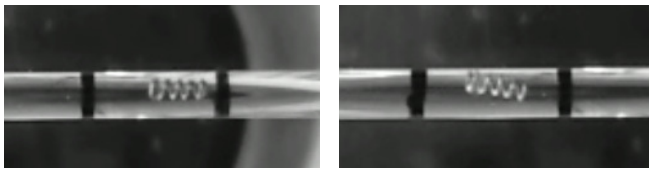

Fig. 11. Snapshots of L2W3 in motion over 3 seconds.

IV. CONCLUSION

We have conducted experiments with magnetically driven micro robots operating in channels with Re < 1. It is observed that motion along the channel depends on the actuation frequency: there exists a safe region where linear change in actuation frequency affects the time-averaged forward velocity proportionally. As the magnetic actuation frequency increases, the magnetic torque cannot overcome the viscous resistance of the fluid. Then, the swimmer cannot rotate with the external magnetic field synchronously, and occasionally stops and even rotates in the opposite direction due to the variations in the instantaneous directions of the magnetic moment of the head and the external magnetic field. Thus forward velocity drops, however, exhibiting a nonlinear behavior. Proposed RFT-based hydrodynamic model predicts the nonlinear decrease in forward velocity after step-out frequency observed as well as the linear relationship in between actuation frequency and time-averaged forward velocity. Normal drag factors of swimmer bodies are tuned to account for the irregularity of its shape and flow conditions for each robot once. Similarly the magnetization of the head is also tuned once for each robot to account for the misalignment between the magnetization vector and the applied magnetic field. Lateral velocities, and thus **yz**-trajectory, are constrained numerically with proper modification of body and tail resistance matrices with respect to swimmer position and orientation in the channel in order to include the near-wall effects of the cylindrical channel.

REFERENCES

[1] J. Edd, S. Payen, B. Rubinsky, M. L. Stoller, and M. Sitti, "Biomimetic propulsion for a swimming surgical micro-robot," *IEEE/RSJ Intelligent Robotics and Systems Conference* (*IROS*), vol.3, pp. 2583-2588, Las Vegas, USA, October 2003.

[2] B. Behkam and M. Sitti, "Design methodology for biomimetic propulsion of miniature swimming robots," *ASME Journal of Dynamic Systems, Measurement, and Control*, vol. 128, no.1, pp. 36-43, March 2006.

[3] S. Martel, "Collective methods of propulsion and steering for untethered microscale nanorobots navigating in the human vascular network," *Journal of Mech. Eng. Science*, pp. 1505-1513, 2010.

[4] B. J. Nelson, I. K. Kaliakatsos, and J. J. Abbott, "Microrobots for minimally invasive medicine," *Annu. Rev. Biomed. Eng.,* vol. 12, pp. 55-85, April, 2010.

[5] L. Zhang, J. J. Abbott, L. Dong, B. E. Kratochvil, D. Bell, and B. J. Nelson, "Artificial bacterial flagella: fabrication and magnetic control," *Applied Physics Letters*, vol. 94, pp. 064107-1-3, February, 2009.

[6] L. Zhang, J. J. Abbott, L. Dong, K. E. Peyer, B. E. Kratochvil, H. Zhang, C. Bergeles, and B. J. Nelson, "Characterizing the swimming properties of artificial bacterial flagella," *Nano Letters,* vol. 9, no. 10, pp. 3663-3667, August 15, 2010.

[7] A. Ghosh and P. Fischer, "Controlled propulsion of artificial magnetic nanostructured propellers," *Nanoletters,* vol. 9, no. 6, pp. 2243-2245, March, 2009.

[8] T. Honda, K. I. Arai, and K. Ishiyama, "Micro swimming mechanisms propelled by external magnetic fields," *IEEE Transactions on Magnetics,* vol. 32, pp. 5085-5087, Sept. 1996.

[9] J. Lighthill, "Flagellar hydrodynamics: the John von Neumann lecture," *SIAM Review*, vol. 18, no. 2, pp. 161-230, April, 1976.

[10] J. Gray and G. J. Hancock, "The propulsion of sea-urchin spermatozoa," *J. Exp. Biol.*, Vol. 32, pp. 802-814, 1955.

[11] C. Brennen and H. Winet, "Fluid mechanics of propulsion by cilia and flagella," *Ann. Rev. Fluid Mech.*, Vol. 9, pp. 339-398, 1977.

[12] J. R. Blake, "Singularities of viscous flow," J. Eng. Math., Vol. 8, No. 2, 1974.

[13] E. Lauga, W. R. DiLuzio, G. M. Whitesides, and H. A. Stone, "Swimming in circles: motion of bacteria near solid boundaries," *Biophysical Journal*, Vol.90, pp. 400-412, 2006.

[14] J.J.L. Higdon, "The hydrodynamics of flagellar propulsion: helical waves," *J. Fluid Mech.*, Vol. 94, No. 2, pp. 331-351, 1979.

[15] B. U. Felderhof, "Swimming at low reynolds number of a cylindrical body in a circular tube," *Phys. of Fluids*, Vol. 22, 1136041-6, 2010.

[16] M. Manghi, X. Schlagberger, and R. R. Netz, "Propulsion with a rotating elastic nanorod," *Physical Review Letters*, Vol. 96, 068101,2006.

[17] R. Dreyfus, J. Baudry, M. L. Roper, M. Fermigier, H.A.Stone, and J. Bibette, "Microscopic artificial swimmers," *Nature,* vol. 437, pp. 862-865, Oct. 2005.

[18] F. Z. Temel and S. Yesilyurt, "Magnetically Actuated Micro Swimming of Bio-inspired Robots in Mini Channels," *IEEE International Conference on Mechatronics*, ITU Taşkışla-Taksim Istanbul, Turkey, April 13-15, 2011.

[19] A. F. Tabak and S. Yesilyurt, "Validated reduced order models for simulating trajectories of bio-inspired artificial micro-swimmers," *FEDSM2010-ICNMM2010, ASME 2010 3rd Joint US-European Fluids Engineering Summer Meeting and 8th International Conference on Nanochannels, Microchannels and Minichannels*, Montreal, Canada, Aug. 2-4, 2010.

[20] A. J. Hanson and H. Ma, "Visualizing flow with quaternion frames," in *Proc. of the conference on Visualization '94*, Washington, D.C., 1994, pp. 108-115.

[21] D. Baraff, "Physical based modeling, rigid body simulation," Course Notes, ACM SIGGRAPH, 2001.

[22] D. Jiles, Introduction to Magnetism and Magnetic Materials, 2nd ed., Ed. London, UK: Chapman & Hall, 1998.

[23] L.F. Shampine and M. K. Gordon, Computer Solution of Ordinary Differential Equations: the Initial Value Problem, W. H. Freeman, SanFrancisco, 1975.